Biomagnetic fluid flow in a driven cavity

E. E. Tzirtzilakis & M. A. Xenos

Meccanica
An International Journal of Theoretical and Applied Mechanics AIMETA

ISSN 0025-6455
Volume 48
Number 1

Meccanica (2013) 48:187-200
DOI 10.1007/s11012-012-9593-7

Springer

Meccanica (2013) 48:187–200
DOI 10.1007/s11012-012-9593-7

Biomagnetic fluid flow in a driven cavity

E.E. Tzirtzilakis · M.A. Xenos

Received: 13 November 2011 / Accepted: 2 August 2012 / Published online: 16 August 2012

Abstract In this study, the fundamental problem of the biomagnetic fluid flow in a lid driven cavity under the influence of a steady localized magnetic field is studied. The mathematical model used for the formulation of the problem is consistent with the principles of Ferrohydrodynamics (FHD) and Magnetohydrodynamics (MHD). The biomagnetic fluid is considered as a homogeneous Newtonian fluid and is treated as an electrically conducting magnetic fluid which also exhibits magnetization. A known biomagnetic fluid which exhibits such magnetic properties is blood. For the numerical solution of the problem, which is described by a coupled, non linear system of PDEs, with appropriate boundary conditions, the SIMPLE algorithm is used. The solution is obtained by the development of a numerical methodology using finite volumes on a staggered, properly stretched, grid. Results concerning the velocity indicate that the presence of the magnetic field influences considerably the flow field.

E.E. Tzirtzilakis (✉)
Department of Mechanical and Water Resources Engineering, Technological Educational Institute of Messolonghi, Messolonghi, 30200, Greece
e-mail: etzirtzilakis@teimes.gr

M.A. Xenos
Department of Mathematics, University of Ioannina, Ioannina, 45110, Greece
e-mail: mxenos@cc.uoi.gr

Keywords Ferrohydrodynamics · Magnetohydrodynamics · Magnetic fluid · Driven cavity · Biomagnetic

1 Introduction

Biomagnetic Fluid Dynamics (BFD) is a new area in fluid mechanics investigating the fluid dynamics of biological fluids in the presence of magnetic field. According to BFD, which was developed by Haik et al. [1, 2], the biological fluids are treated as isothermal, Newtonian, electrically non conducting magnetic fluids. This model is consistent with the principles of Ferrohydrodynamics (FHD) [3–9] and the dominant force in the flow field is that of magnetization. A characteristic biomagnetic fluid is blood. Blood exhibits polarization due to the erythrocytes which constitute magnetic dipoles in a liquid carrier (plasma) [1].

An extended BFD mathematical model, was developed by Tzirtzilakis [10]. The two basic differences with the initial BFD model of Haik et al. are the following. First, the biofluid is not considered isothermal and the temperature distribution is studied in the flow field. Second, biofluid is considered to be electrically conducting whereas, at the same time the polarization forces are taken into account [10]. These modifications were adopted due to the fact that blood, for strong magnetic fields, behaves like an electrically conducting fluid which simultaneously exhibits magnetization. Consequently, the latter BFD model incorporates

the principles of Magnetohydrodynamics (MHD) [11–14] along with the principles of FHD and the dominant forces in the flow field are both magnetization and the Lorentz force [10]. Under certain assumptions, as far as the applied magnetic field is concerned, e.g. sharp magnetic field gradient or low magnetic field strength, the momentum equations of [10] can be reduced to that used in the BFD model of Haik et al. [1, 2, 10].

As far as the applications are concerned, a usual technique is the addition to blood of artificially created nano-particles. These particles either are attached to erythrocytes, or they are moving independently in blood. This practically means that the magnetization of blood is increased by orders of magnitude and blood behaves like a ferromagnetic fluid. The afore mentioned technique is used for targeted transport of drugs using magnetic particles as drug carriers, reduction of bleeding during surgeries or provocation of occlusion of the feeding vessels of cancer tumors and development of magnetic tracers. Moreover, biomedical applications are proposed with the application of magnetic field directly on blood. Among them is the development of magnetic devices for cell separation and magnetic wound treatment or cancer tumor treatment causing magnetic hyperthermia [15–23].

Numerical studies concerning basic flow configurations such as the BFD channel flow using the BFD model of Haik et al. [1] were investigated in [24]. The primary effect is the formation of a vortex at the area of the application of the magnetic field. Similar basic flow configurations were also investigated in BFD flow problems considering non-Newtonian behavior of the biofluid [25–30]. Furthermore, it has been observed from the procedure of the numerical solution of BFD problems that the magnetization term introduced in the governing equations, multiplied by the Mn_F number (which is of the order of 10^2–10^3), constitutes a dense "source term" leading in extended disturbances in the flow field like the formation of vortices. This "source" generates numerical instabilities and divergence and leads to the need for seeking methodologies and techniques which improve the stability characteristics of the used numerical method. One such technique seem to be the stretching of the grid used also in [10] and [31].

One of the most well known classical fundamental problems is that of the driven lid cavity. One of the most well known papers on the lid-driven cavity is that of Ghia et al. [32]. Although this physical problem is one of the first investigated it is the most famous as a benchmark problem for numerical algorithms and papers are still publishing [33–35].

One of the most common methodologies for the numerical treatment of incompressible fluid flow problems, like the ones arising also in BFD, is the adoption of the stream function-vorticity (or velocity-vorticity) formulation. Such a treatment was used for the lid-driven cavity in [33–35] and for BFD channel flows in [24] and [31].

As far as the physical problem of magnetic fluid flow is concerned, interesting physical problems have also been investigated in [36–40]. The ferrofluid flow in a cavity has been investigated in [41]. The square cavity was considered to have two opposite sides at two different temperatures and the other two (top and bottom) insulated. All the walls were still. It was derived that flow arises by the application of the magnetic field and it is strengthened as the magnetic field increases. Analysis has also been made for the side wall heat transfer and the thermal convection in the flow field. The same physical problem was recently investigated in [42]. Furthermore, the isothermal MHD flow in a lid-driven cavity was investigated in [43]. For the numerical solution the stream function vorticity formulation was used and the analysis showed great influence of the vortices in the flow field by the arising Lorentz force. The form (penetration parameter) and the magnetic field strength (Stuart number) seemed to be the factors of controlling the generation, shape and size of the vortices in the lid-driven cavity.

In the present study, the BFD flow in a lid-driven cavity is numerically investigated. The flow is assumed to be isothermal, two dimensional, laminar, incompressible and the magnetization is described by a linear equation involving the magnetic intensity H. The mathematical model of [10] is taken into account, and consequently, the biofluid is blood which is considered as a homogeneous, Newtonian and electrically conducting ferrofluid sustained equilibrium magnetization [10, 24, 31]. The physical problem is described by a coupled, non linear system of partial differential equations (PDEs) resulting from the mathematical model presented in [10]. The solution of the problem is obtained numerically by the development of an efficient numerical methodology based on the SIMPLE algorithm.

The results presented concerning the velocity and skin friction on the side walls, show that the flow is

appreciably influenced by the application of the magnetic field. The generation as well as the shape of the vortices in the flow field depend on the magnetic field strength intensity. These encouraging results indicate that the application of a magnetic field, in the flow of biomagnetic fluid, could be useful for medical and engineering applications.

2 Mathematical formulation and numerical methodology

2.1 Mathematical description of the problem

The viscous, steady, two-dimensional, incompressible, laminar biomagnetic fluid (blood) flow is considered taking place in a lid driven cavity. The length of the plates is $\bar{L}$ and the cavity is square. The flow is subject to a magnetic source, which is placed very close to the lower plate of the cavity and below. This magnetic source is actually a point source (in 2D) or the magnetic field arising from a line current perpendicular to the cavity. A schematic representation of the flow field as well as the magnetic field strength contours are given in Fig. 1(A). The origin of the Cartesian coordinate system is located at the leading edge of the lower plate, i.e. the origin of the Cartesian system is at the bottom left corner of the cavity.

For the biomagnetic fluid (blood) as well as for the flow, all the assumptions of the mathematical model proposed in [10] are made. Namely, blood is considered to be an electrically conducting Newtonian magnetic fluid exhibiting paramagnetic behavior. The flow is considered to be laminar and the increment of the viscosity due to the magnetic field is considered to be negligible. The rotational forces acting on the erythrocytes, when entering and exiting the magnetic field are discarded (equilibrium magnetization). Finally, the flow is considered isothermal and the electric field is considered negligible since the flow is two dimensional.

Under the above assumptions the equations governing the flow under consideration are [10]:

$$\frac{\partial \bar{u}}{\partial \bar{x}} + \frac{\partial \bar{v}}{\partial \bar{y}} = 0, \tag{1}$$

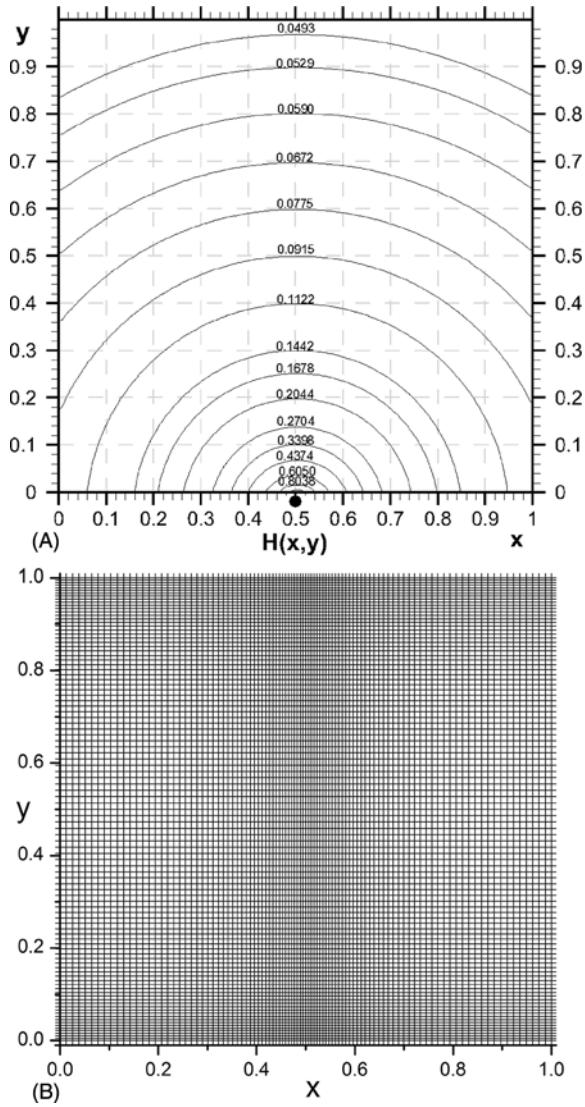

Fig. 1 (**A**): Dimensionless magnetic field strength contours. Variations from $H(0.5, 0) = 1$. (**B**): Grid configuration

$$\bar{\rho}\left(\bar{u}\frac{\partial \bar{u}}{\partial \bar{x}} + \bar{v}\frac{\partial \bar{u}}{\partial \bar{y}}\right) = -\frac{\partial \bar{p}}{\partial \bar{x}} + \bar{\mu}_0 \bar{M}\frac{\partial \bar{H}}{\partial \bar{x}} - \bar{\sigma}\bar{B}_y^2 \bar{u} + \bar{\sigma}\bar{B}_x \bar{B}_y \bar{v} + \bar{\mu}\left(\frac{\partial^2 \bar{u}}{\partial \bar{x}^2} + \frac{\partial^2 \bar{u}}{\partial \bar{y}^2}\right), \tag{2}$$

$$\bar{\rho}\left(\bar{u}\frac{\partial \bar{v}}{\partial \bar{x}} + \bar{v}\frac{\partial \bar{v}}{\partial \bar{y}}\right) = -\frac{\partial \bar{p}}{\partial \bar{y}} + \bar{\mu}_0 \bar{M}\frac{\partial \bar{H}}{\partial \bar{y}} - \bar{\sigma}\bar{B}_x^2 \bar{v} + \bar{\sigma}\bar{B}_x \bar{B}_y \bar{u} + \bar{\mu}\left(\frac{\partial^2 \bar{v}}{\partial \bar{x}^2} + \frac{\partial^2 \bar{v}}{\partial \bar{y}^2}\right). \tag{3}$$

The boundary conditions of the problem are

$$\left.\begin{array}{ll}\text{Upper Wall} & (\bar{y}=\bar{L},\ 0\le\bar{x}\le\bar{L}):\\ & \bar{u}=\bar{u}_r,\ \bar{v}=0.\\ \text{Lower Wall} & (\bar{y}=0,\ 0\le\bar{x}\le\bar{L}):\\ & \bar{u}=0,\ \bar{v}=0.\\ \text{Left Wall} & (\bar{x}=0,\ 0\le\bar{y}\le\bar{L}):\\ & \bar{u}=0,\ \bar{v}=0.\\ \text{Right Wall} & (\bar{x}=\bar{L},\ 0\le\bar{y}\le\bar{L}):\\ & \bar{u}=0,\ \bar{v}=0.\end{array}\right\} \tag{4}$$

In the above equations $\vec{q}=(\bar{u},\bar{v})$ is the dimensional velocity, $\bar{p}$ is the pressure, $\bar{u}_r$ is a constant velocity, $\bar{\rho}$ is the biomagnetic fluid density, $\bar{\sigma}$ is the electrical conductivity, $\bar{\mu}$ is the dynamic viscosity, $\bar{\mu}_o$ is the magnetic permeability of vacuum, $\vec{H}=(\bar{H}_x,\bar{H}_y)$ is the magnetic field strength, $\vec{B}$ is the magnetic induction ($\vec{B}=\mu_0\vec{H}\Rightarrow(\bar{B}_x,\bar{B}_y)=\mu_0(\bar{H}_x,\bar{H}_y)$) and the bar above the quantities denotes that they are dimensional.

The terms $\bar{\mu}_o\bar{M}\partial\bar{H}/\partial\bar{x}$ and $\bar{\mu}_o\bar{M}\partial\bar{H}/\partial\bar{y}$ in (2) and (3), respectively, represent the components of the magnetic force, per unit volume, and depend on the existence of the magnetic gradient on the corresponding x and y directions. These two terms are well known from FHD [3–9]. The terms $-\bar{\sigma}\bar{B}_y^2\bar{u}+\bar{\sigma}\bar{B}_x\bar{B}_y\bar{v}$ and $-\bar{\sigma}\bar{B}_x^2\bar{v}+\bar{\sigma}\bar{B}_x\bar{B}_y\bar{u}$ appearing in (2) and (3), respectively, represent the Lorentz force per unit volume towards the x and y directions and arise due to the electrical conductivity of the fluid. These two terms are known in MHD [11–14]. The principles of MHD and FHD are combined in the mathematical model presented in [10] and the above mentioned terms arise together in the governing equations (2) and (3).

For the variation of the magnetization $\bar{M}$, with the magnetic field intensity $\bar{H}$, experiments which has been carried out in [2] showed that it can be fairly approximated by the linear relation [10]

$$\bar{M}=\bar{\chi}\bar{H}, \tag{5}$$

where $\bar{\chi}$ is a constant called magnetic susceptibility. In the above relation, the components of the magnetic field intensity $\bar{H}_x$ and $\bar{H}_y$ along the $\bar{x}$ and $\bar{y}$ coordinates, ($\vec{H}=(\bar{H}_x,\bar{H}_y)$) are given respectively by

$$\begin{aligned}\bar{H}_x&=\frac{\gamma}{2\pi}\frac{\bar{y}-\bar{b}}{(\bar{x}-\bar{a})^2+(\bar{y}-\bar{b})^2},\\ \bar{H}_y&=-\frac{\gamma}{2\pi}\frac{\bar{x}-\bar{a}}{(\bar{x}-\bar{a})^2+(\bar{y}-\bar{b})^2}\end{aligned} \tag{6}$$

where $(\bar{a},\bar{b})$ is the point where the magnetic source is placed and γ is the magnetic field strength at this point ($\bar{x}=\bar{a}$, $\bar{y}=\bar{b}$).

The magnitude $\bar{H}$, of the magnetic field intensity, is given by

$$\begin{aligned}\bar{H}(\bar{x},\bar{y})&=\left[\bar{H}_x^2+\bar{H}_y^2\right]^{1/2}\\ &=\frac{\gamma}{2\pi}\frac{1}{\sqrt{(\bar{x}-\bar{a})^2+(\bar{y}-\bar{b})^2}}.\end{aligned} \tag{7}$$

2.2 Transformation of the equations

In order to proceed to the numerical solution of the system (1)–(3) with the boundary conditions (4) and the assumptions (5) and (7), the following non dimensional variables are introduced

$$x=\frac{\bar{x}}{\bar{L}},\qquad y=\frac{\bar{y}}{\bar{L}},\qquad u=\frac{\bar{u}}{\bar{u}_r},\qquad v=\frac{\bar{v}}{\bar{u}_r}, \tag{8}$$

$$p=\frac{\bar{p}}{\rho\bar{u}_r^2},\qquad H_x=\frac{\bar{H}_x}{\bar{H}_o},\qquad H_y=\frac{\bar{H}_y}{\bar{H}_o} \tag{9}$$

where $\bar{H}_o=\bar{H}(\bar{a},0)$.

By substitution of (8) and (9) to Eqs. (1)–(3) and taking into account (5), the following system of equations is derived

$$\frac{\partial u}{\partial x}+\frac{\partial v}{\partial y}=0, \tag{10}$$

$$\begin{aligned}u\frac{\partial u}{\partial x}+v\frac{\partial u}{\partial y}=&-\frac{\partial p}{\partial x}+Mn_F H\frac{\partial H}{\partial x}\\ &-N\left(uH_y^2-vH_xH_y\right)\\ &+\frac{1}{Re}\left(\frac{\partial^2 u}{\partial x^2}+\frac{\partial^2 u}{\partial y^2}\right),\end{aligned} \tag{11}$$

$$\begin{aligned}u\frac{\partial v}{\partial x}+v\frac{\partial v}{\partial y}=&-\frac{\partial p}{\partial y}+Mn_F H\frac{\partial H}{\partial y}\\ &-N\left(vH_x^2-uH_xH_y\right)\\ &+\frac{1}{Re}\left(\frac{\partial^2 v}{\partial x^2}+\frac{\partial^2 v}{\partial y^2}\right)\end{aligned} \tag{12}$$

The boundary conditions of the problem are

$$\left.\begin{array}{ll}\text{Upper Wall} & (y=1,\ 0\le x\le 1):\\ & u=1,\ v=0.\\ \text{Lower Wall} & (y=0,\ 0\le x\le 1):\\ & u=0,\ v=0.\\ \text{Left Wall} & (x=0,\ 0\le y\le 1):\\ & u=0,\ v=0.\\ \text{Right Wall} & (x=1,\ 0\le y\le 1):\\ & u=0,\ v=0.\end{array}\right\} \tag{13}$$

The non-dimensional parameters entering now into the problem under consideration are

$$Re = \frac{\bar{L}\bar{\rho}\bar{u}_r}{\bar{\mu}} \quad \text{(Reynolds number)},$$

$$N = \frac{\bar{\mu}_o^2 \bar{H}_o^2 \bar{L}\bar{\sigma}}{\bar{\rho}\bar{u}_r} = \frac{Ha^2}{Re} \quad \text{(Stuart number)}.$$

$$Mn_F = \frac{\bar{\mu}_o \bar{\chi} \bar{H}_o^2}{\bar{\rho}\bar{u}_r^2}$$

(Magnetic number arising from FHD).

The parameter entering into the problems of BFD (and consequently of FHD) is the magnetic number Mn_F defined above. The parameter, N, is the Stuart number which is the ratio of the square of the Hartman number to the Reynolds number [11–14]. It is worth mentioning here that when both of these magnetic numbers are zero, the problem is reduced to the problem of a common hydrodynamic flow in driven lid cavity. When Mn_F is set to zero then the problem is reduced to the MHD driven lid cavity flow whereas, when N is set to zero the problem is reduced to a FHD driven lid cavity flow. For a specific Reynolds number, increasing these magnetic numbers is equivalent to increasing the magnetic field strength $\bar{H}_o$.

The magnitude H, of the magnetic field intensity, is also derived by the relations (7), (8) and (9) and is given by the relation

$$H(x, y) = \frac{|b|}{\sqrt{(x-a)^2 + (y-b)^2}}. \tag{14}$$

2.3 Numerical method

For the numerical solution of the system of Eqs. (10)–(12) subject to the boundary conditions (13), an efficient technique is developed. In this technique, the finite volume method on a staggered, properly stretched, grid was used for discretizing the non linear set of equations. For the numerical solution of the problem the SIMPLE algorithm was used.

2.3.1 Grid configuration

For the present physical problem, calculations where performed testing different forms of grid stretching also used in [10] and [31]. The grid used can be described as a result of transformations. Let $(\xi - \eta)$ be the plane where a uniform grid is defined and a transformation taking place between the planes $(x - y)$ and $(\xi - \eta)$. According to this transformation the grid is stretched to a way that is more dense towards the horizontal walls (y-direction) and to the $x = a$ point (x-direction) where the magnetic field is applied.

The relation between the coordinates is given below [44]:

$$\begin{aligned} x &\equiv x(\xi) = \xi_o \left(1 + \frac{\sinh[\tau(\xi - \lambda)]}{\sinh[\tau\lambda]}\right), \\ y &\equiv y(\eta) = \frac{2\delta_1 - \delta_2 + (\delta_2 + 2\delta_1)\kappa_1^{\frac{\eta-\delta_1}{1-\delta_1}}}{(1 + 2\delta_1)(1 + \kappa_1^{\frac{\eta-\delta_1}{1-\delta_1}})}, \end{aligned} \tag{15}$$

$$\xi \equiv \xi(x) = \lambda + \frac{1}{\tau}\sinh^{-1}\left[\left(\frac{x}{\xi_o} - 1\right)\sinh(\lambda\tau)\right], \tag{16}$$

$$\eta \equiv \eta(y) = \delta_1 + \frac{(1 - \delta_1)\ln[\kappa_2]}{\ln[\kappa_1]}$$

where

$$\lambda = \frac{1}{2\tau}\ln\left|\frac{1 + (e^{\tau} - 1)(\xi_o/\xi_{\max})}{1 + (e^{-\tau} - 1)(\xi_o/\xi_{\max})}\right|, \tag{17}$$

$$\kappa_1 = \left(\frac{\delta_2 + 1}{\delta_2 - 1}\right), \qquad \kappa_2 = \frac{-2\delta_1 + \delta_2 + y(1 + 2\delta_1)}{2\delta_1 + \delta_2 - y(1 + 2\delta_1)}.$$

In the above relations, $\xi_{\max}$ is the dimensionless length of the cavity which is 1 for the present case, ξ_o is the point where the grid clustering occurs, which for the present case is $\xi_o = a$. The parameter τ is controlling the rate of clustering towards the x direction and varies from zero (no stretching) to large values that produce the biggest clustering near $\xi = \xi_o$. Moreover, δ_1 and δ_2 are parameters controlling the stretching towards the y direction. If $\delta_1 = 0$, then the mesh will be refined only near $y = 1$ whereas, if $\delta_1 = 0.5$, the mesh will be refined equally near $y = 0$ and $y = 1$ [44]. Thus, the grid is clustered towards the x direction at the area of the magnetic source. A clustering occurs also near the horizontal walls due to the stretching towards the y direction. A representative grid configuration, for $\delta_1 = 0.5$ is shown at Fig. 1B. It is observed, that the use of this stretched grid slightly improves the stability characteristics of the used numerical method. The results presented in this study have also been compared with others derived using uniform grid and no differences were found.

2.3.2 Numerical scheme

A staggered grid arrangement was used in our approach, offering advantages over the collocated arrangement especially in convective dominated flows

[45]. Instead placing all variables in one grid, different variables are placed on different grids, which are shifted half a grid point. In addition to the stagger grid approach, an appropriate stretching of the grid was applied where close to the walls the computational grid was finer and became coarser close to the center of the driven cavity domain (discussed in previous section). This is due to the fact that more action is taking place close to the area of the magnetic source [10].

The upwind scheme is introduced to the discretized equations to overcome problems concerning high convection terms in the momentum. With this formulation the influence of the convection terms was minimized retaining the diffusion terms unchanged as the velocity increases in the flow field. Upwind scheme provides a first order accuracy instead of second order that the diffusion terms retain, leading to inaccurate solution when the local velocity gradients are large. To overcome this problem the "deferred correction" approach was utilized [46]. In this scheme higher-order flux approximations (central difference scheme) are computed explicitly and this approximation is combined with implicit low-order approximations (upwind difference scheme) [46]. More accurate solution could be obtained utilizing higher order schemes [47].

The Semi-Implicit Method for Pressure Linked Equations (SIMPLE) was used to solve the system of the momentum and pressure correction equations. In this method a guess-correct philosophy was employed that gradually improves the guessed solution by repeated use of the discrete governing equations [48]. In SIMPLE could be challenging to choose the under relaxation factors since these factors are problem specific. In this case the relaxation factors used for the momentum equations where equal to 0.8 where for the pressure correction equations was equal to 0.2. More details about the SIMPLE algorithm can be found elsewhere [46, 48].

2.4 Assignment of the parameter values

The above described numerical technique was applied to solve the system of Eqs. (10)–(12), under the appropriate boundary conditions (13). In order to proceed to the derivation of the numerical results, it is necessary to assign values to the dimensionless parameters entering the problem under consideration. A representative case of a physical problem is considered and a methodology is presented for the derivation of the values of the dimensionless parameters. A case scenario similar to that adopted in [24] and [31] is considered in which the fluid is blood ($\bar{\rho} = 1050\ \mathrm{kg\,m^{-3}}$, $\bar{\mu} = 3.2 \times 10^{-3}\ \mathrm{kg\,m^{-1}\,s^{-1}}$) [49]. The velocity of the lid can be chosen to be $\bar{u}_r = 2.438 \times 10^{-2}\ \mathrm{m\,s^{-1}}$ and the length of the plates of the cavity $\bar{L} = 5.0 \times 10^{-2}$ m, whereas the magnetic source is placed at distance $\bar{b} = 2.5 \times 10^{-3}$ m from the cavity. Hence $b = 0.05$ and the Reynolds number, Re, is equal to 400. The dimensionless parameter appearing in the BFD flow problem is the magnetic number Mn_F and it can be written as

$$Mn_F = \frac{\bar{\mu}_o \bar{H}_o^2 \bar{\chi}}{\bar{\rho}\bar{u}_r^2} = \frac{\bar{\mu}_o \bar{H}_o \bar{\chi}\, \bar{H}_o}{\bar{\rho}\bar{u}_r^2} = \frac{\bar{B}_o \bar{M}_o}{\bar{\rho}\bar{u}_r^2} = \frac{\bar{M}_o \bar{B}_o \bar{L}^2 \bar{\rho}}{\bar{\mu}^2 Re^2}, \tag{18}$$

where $\bar{B}_o$ and $\bar{M}_o$ are the magnetic induction and the magnetization at the point $(a, 0)$, respectively. The quantity $\bar{u}_r$ at the last equality of the above relation has been replaced using the definition of the Reynolds number $\bar{u}_r = \bar{\mu} Re / \bar{L}\bar{\rho}$.

A first estimation of a potential value of Mn_F can be made using a reference magnetic field of 8 Tesla. For such a strong magnetic field, blood has reached saturation magnetization of 40 $\mathrm{A\,m^{-1}}$ [2]. However, the range of realistic values of Mn_F can be very large and quite unpredictable, even for magnetic field strengths of the order of 1 T, due to reasons discussed in detail in [31]. Thus, by assuming that saturation magnetization $M_o = 40\ \mathrm{A\,m^{-1}}$ is attained, it is possible to produce a relation, which gives realistic range of values for the Mn_F related to the applied magnetic field B_o and the Re number. Analogous procedure for Mn_F was also used in [10, 24] and [31]. Substitution of the values considered in the present case scenario, relation (18) gives

$$Mn_F = \frac{1.0253906 \cdot 10^7 B_o}{Re^2}. \tag{19}$$

Blood particularly, exhibits considerably high static electrical conductivity which depends on the hematocrit and the temperature. The electrical conductivity $\bar{\sigma}$ of stationary blood was measured to be 0.7 $\mathrm{S\,m^{-1}}$ [50]. The electrical conductivity of flowing blood is always greater than that of the stationary. The increment for medium shear rates is about 10 % and increases with the increment of the hematocrit [51]. In the current study the electrical conductivity of blood is assumed, for simplicity, temperature independent, and

equal to 0.8 S m^{-1} as in [10]. Consequently, the Stuart number (N) is calculated using the relation

$$N = \frac{\bar{\sigma}\bar{\mu}_0^2\bar{H}_0^2\bar{L}}{\bar{\rho}\bar{u}_r} = \frac{\bar{\mu}}{\bar{L}\bar{\rho}\bar{u}_r}\frac{\bar{L}^2\bar{\sigma}\bar{B}_0^2}{\bar{\mu}} = \frac{Ha^2}{Re} = 0.625\frac{B_o^2}{Re}. \quad (20)$$

A typical value for the square of the Hartman number using the above mentioned values of the parameters is $Ha^2 = 40$. The corresponding values of N are calculated in accordance with the Re number. Thus for $Re = 400$ it is obtained that $N = 0.1$.

Using the relations (19) and (20), we are able to derive corresponding values for the parameters Mn_F and N for a specific Re number and for an imposed reference magnetic field strength B_o. It should be stressed that the above mentioned methodology for calculating Mn_F and N is not uniquely defined. Especially Mn_F, Eq. (19), could have much wider range of values due to currently evolving experimental techniques which permit great increment of magnetization (for a given magnetic field strength) by addition of artificially created biocompatible nanoparticles [23, 31]. On the other hand, there are no reported techniques for increasing the electrical conductivity of a biofluid like blood. Thus, the range of values for N derived by the use of relation (20) is considered sufficiently accurate.

3 Results and discussion

Initially, some verification calculations were performed for the hydrodynamic case ($Mn_F = N = 0$). For this case, the governing equations along with the boundary conditions, describe the classical physical problem of the driven lid cavity, for which there are extensive published results in literature [33–35]. In the present paper, several calculations were performed for code validation purposes and only some characteristic results, compared to those of Ghia et al. [32], are presented.

Figure 2 represents result for the hydrodynamic lid driven cavity flow for $Re = 400$. As already mentioned, there are numerous published results concerning the hydrodynamic case. However the majority of the results have been obtained by the use of stream function vorticity formulation and the graphical representations concern the stream function. In the present case the solution is obtained in the form of the u and

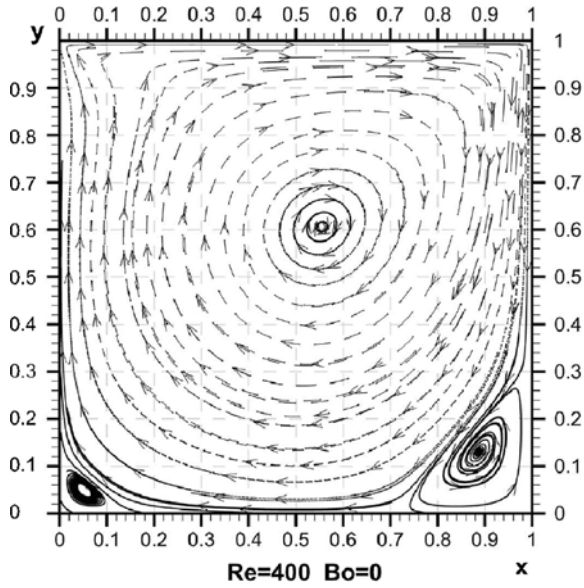

Fig. 2 Streamtraces for $Re = 400$ for pure hydrodynamic flow. This result is in good agreement with the corresponding one in Ghia et al. [32]

v velocities. Thus, the flow field is represented using the "streamtraces" obtained by the velocity field with the use of the software Tecplot 360©. Moreover, streamtraces give additional information for the velocity field. When a streamtrace is continuous, the corresponding velocity is lower than that represented from a streamtrace which is discontinuous. The sparser line of a streamtrace means quicker moving fluid. For steady flows like this, streamtraces are the path an imaginary massless particle would take if it were released into the flow. For vector fields that do not vary over time, streamlines, and streamtraces and massless particle paths are exactly the same thing. On the other hand, the representation of the stream traces is much simpler than that of a velocity field which became very complicated and hard to understand for complex flow patterns. The velocity field presented in Fig. 2 corresponds to $Re = 400$ and consists of a major vortex and two secondary ones at the lower corners. This velocity field is identical to previously obtained numerical results presented at Fig. 3 of [32].

Figure 3 picture results for the classical center u and v velocities, respectively, compared with those derived in Ghia et al. [32]. It is apparent that the agreement is excellent for all the range of Re numbers tested (100–5000). Calculations have been made for grid independent results. The grid sizes used are

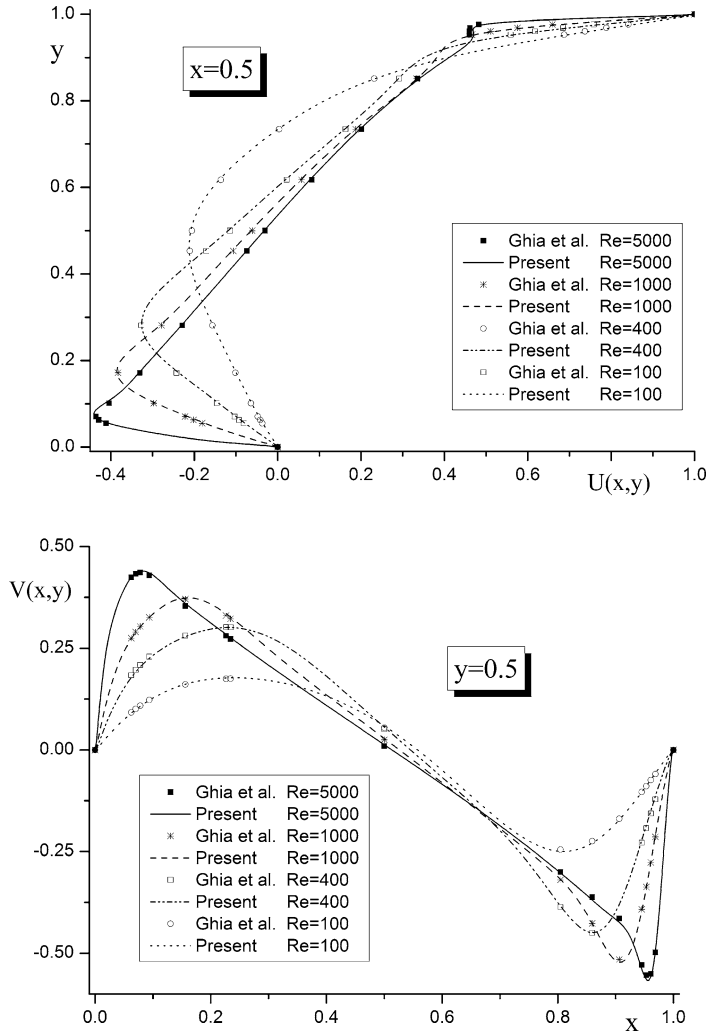

Fig. 3 Comparisons for the u and v center velocities. (*Top*) Profiles of the horizontal velocity at $x = 0.5$. (*Bottom*) Profiles of the vertical velocity along a horizontal section at $y = 0.5$

101×101–301×301. The grid used for the calculations in the present paper is 151×151 and the results have no significant differences with the results obtained using denser grids.

Figure 1(A) represents the magnetic field strength contours. For the results presented, the magnetic source is placed at the point $(0.5, -0.05)$ of the Cartesian system. The reference magnetic field Bo is defined as the magnetic field induction at the point $(0.5, 0)$, i.e. $B_o = B(0.5, 0)$. The dimensionless magnetic field strength intensity $H(0.5, 0) = 1$.

The following results are presented in three sets. Each set consists of three figures (A), (B) and (C) which correspond to the flow pattern generated by the application of reference magnetic field induction of $B_o = 1, 4$, and 8 T, respectively. Figure 4 picture results applying the general BFD model. Figure 5 corresponds to results applying the FHD model by setting $N = 0$ at the governing equations (10)–(12) and finally, Fig. 6 picture results corresponding to MHD by setting $Mn_F = 0$.

The flow field streamtraces for $Re = 400$, $Mn_F = 64.09$ and $N = 1.56 \times 10^{-3}$ is presented at Fig. 4(A). The values of these magnetic parameters correspond to a reference imposed magnetic field induction of $B_o = 1$ T. The flow field now is characterized by the existence of three major and five minor vortices. It is observed that the primary vortex is suppressed towards

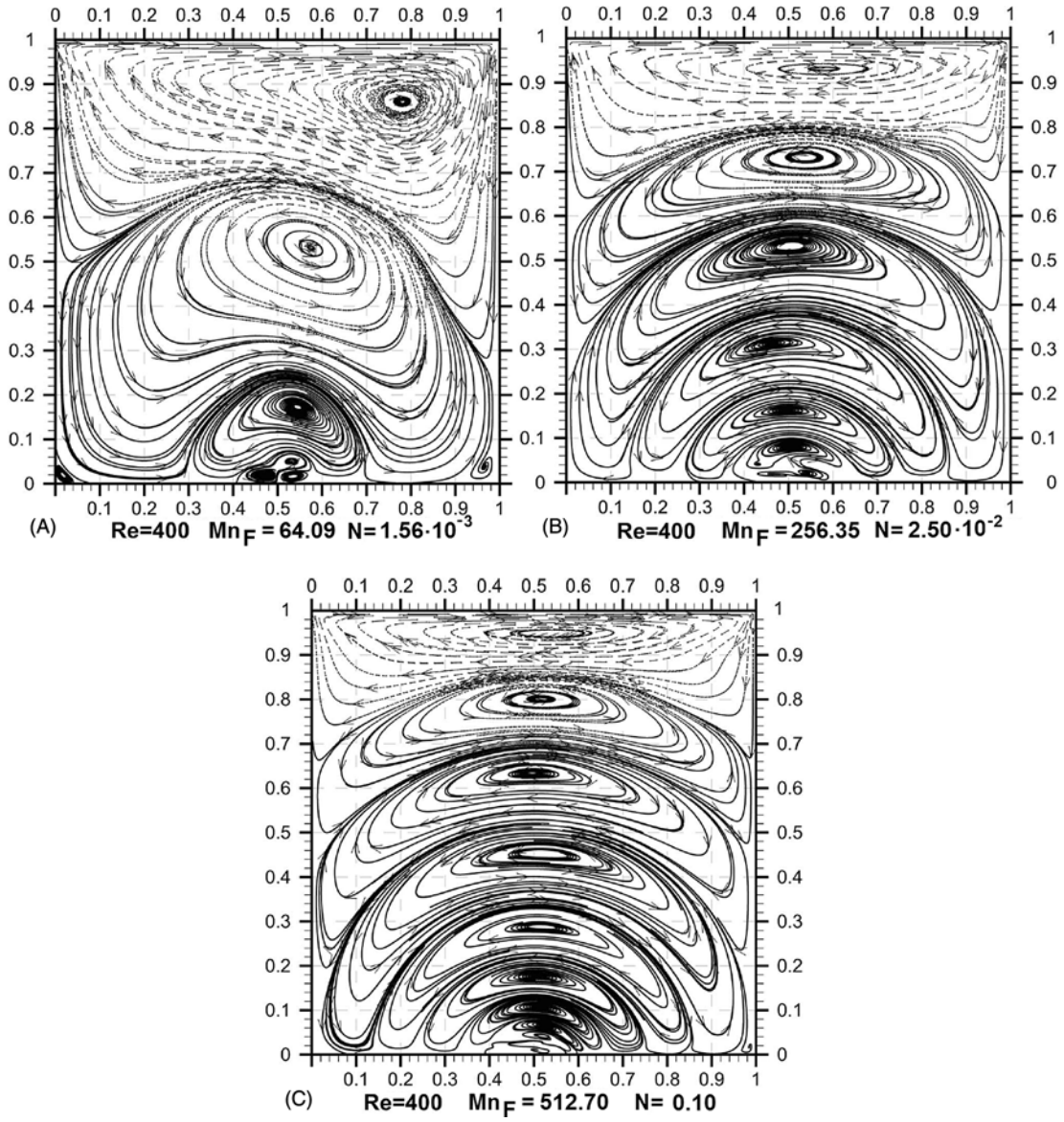

Fig. 4 Streamtraces for $Re = 400$, and various values of Mn_F and N corresponding for reference magnetic field induction of $B_o = 1$, 4, and 8 T, respectively

the upper plate. The center of this clockwise rotating vortex is approximately at the point (0.78, 0.86). The other generated counterclockwise rotating major vortex has center approximately at the point (0.58, 0.53) whereas, the third smaller one at the point (0.54, 0.17). This latter vortex is again rotating clockwise. From this figure it is also obtained that the initial two minor vortices at the lower corners appearing at the pure hydrodynamic flow (Fig. 2), tend to diminish by the application of the magnetic field. The decrement is greater for the vortex at the bottom right corner which from the area $x \gtrsim 0.7$ and $y \lesssim 0.3$ is restricted to the area $x \gtrsim 0.92$ and $y \lesssim 0.8$ by the application of the magnetic field. Finally, three minor vortices appear close to the area of the magnetic source and specifically for $0.4 \lesssim x \lesssim 0.6$ and for $0 \lesssim y \lesssim 0.8$.

Figure 4(B) shows the streamtraces for $Re = 400$, $Mn_F = 256.35$ and $N = 2.50 \times 10^{-2}$. For this case six vortices are formed with centers approximately at the points (0.58, 0.93), (0.54, 0.73), (0.50, 0.53),

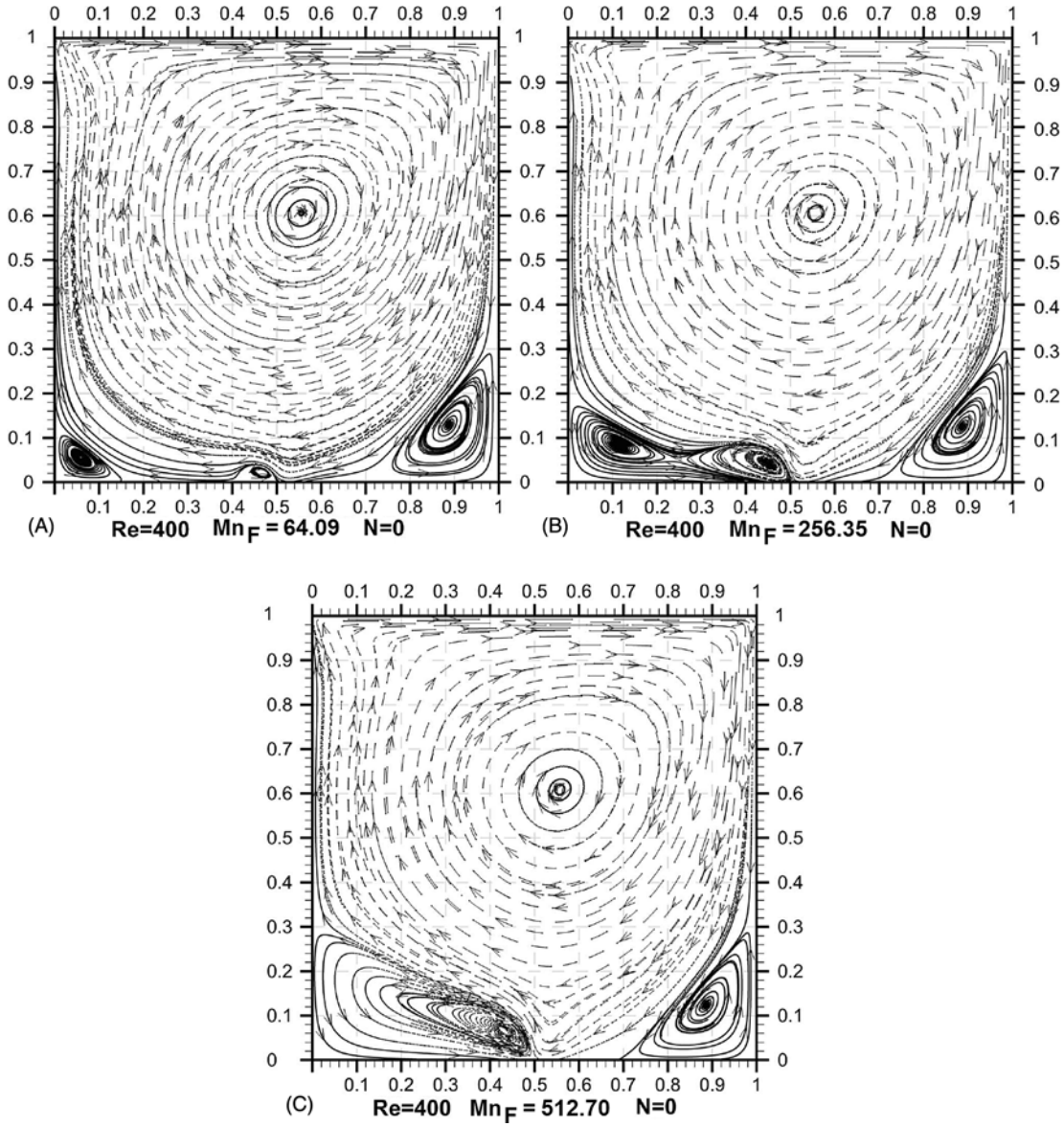

Fig. 5 Streamtraces for $Re = 400$, various values of Mn_F and $N = 0$ (pure FHD flow) corresponding for reference magnetic field induction of $B_o = 1, 4$, and $8T$, respectively

$(0.45, 0.31)$, $(0.5, 0.16)$ and $(0.50, 0.08)$ from the upper to the bottom plate, respectively. Their rotation also changes from clockwise to counterclockwise successively from the upper to the bottom vortex. Close to the area of the magnetic source the fluid is almost stagnant and two minor vortices are barely distinguished at the area $0.44 \lesssim x \lesssim 0.6$ and $y \lesssim 0.3$.

The streamtraces for $Re = 400$, $Mn_F = 512.70$ and $N = 0.10$ are presented at Fig. 4(C). These values of the magnetic parameters correspond to a reference magnetic field of $B_o = 8$ T. The flow field is analogous to the previous case. It is observed that the increment of the magnetic field intensity results to the increment of the number of the formed vortices. For this case seven clearly distinguished vortices are formed with centers approximately at the points $(0.54, 0.95)$, $(0.51, 0.80)$, $(0.50, 0.63)$, $(0.52, 0.45)$, $(0.52, 0.29)$, $(0.51, 0.18)$ and $(0.51, 0.10)$ from top to bottom, respectively. The rotation of the vortices changes, as previously, successively from clockwise to counterclock-

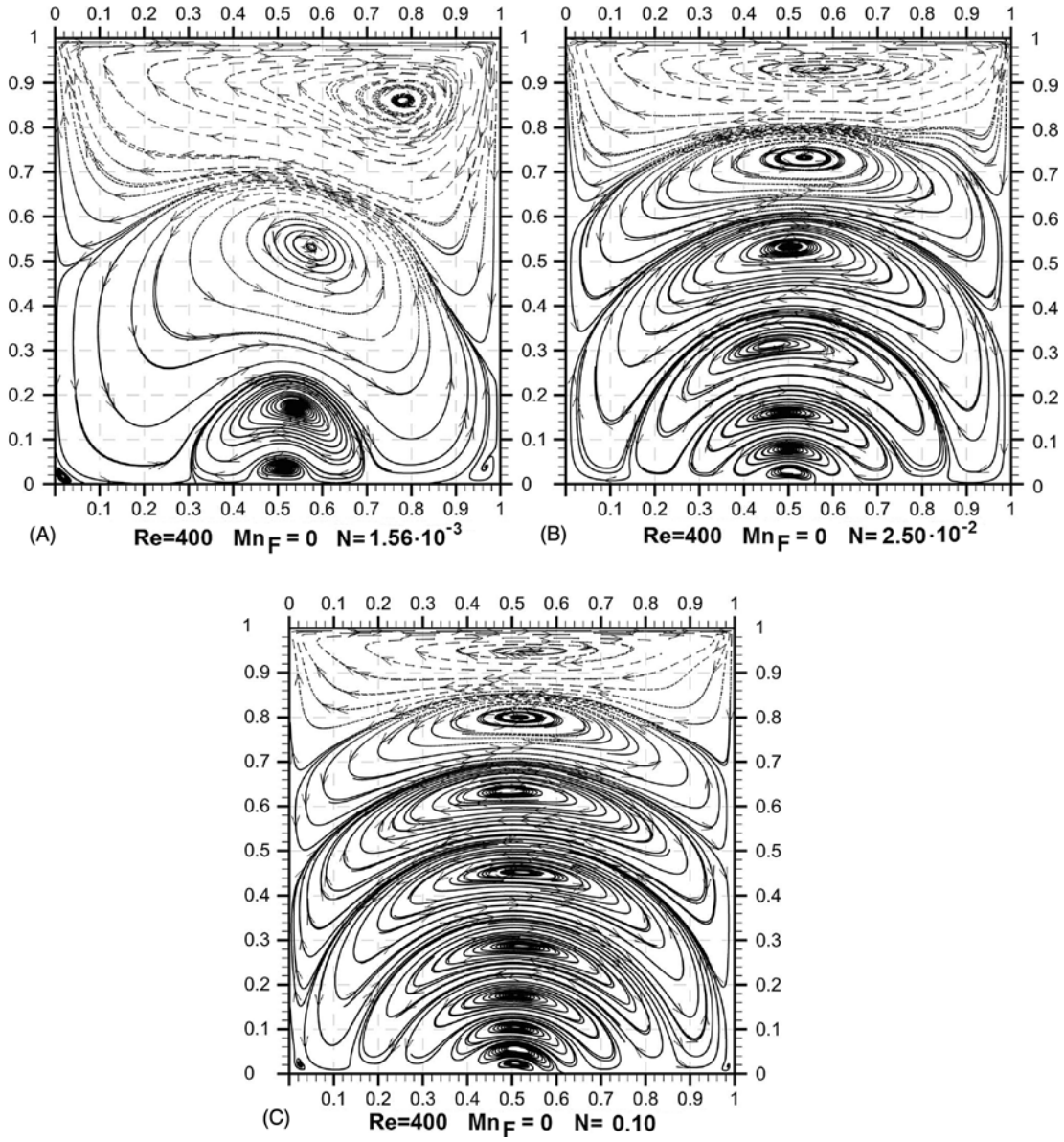

Fig. 6 Streamtraces for $Re = 400$, various values of N and $Mn_F = 0$ (pure MHD flow) corresponding for reference magnetic field induction of $B_o = 1$, 4, and 8 T, respectively

wise from the upper to the bottom vortex. There is also a minor vortex with center approximately at the point (0.53, 0.06). Lower to this point and close to the magnetic source the fluid is again almost stagnant. As a general observation, it can be concluded that the application of a stronger magnetic field makes the flow pattern almost symmetric with respect to the line $x = 0.5$.

As already mentioned in Sect. 2.2, it is possible to investigate either FHD or MHD driven lid cavity flow problems by setting N or Mn_F zero, respectively at the governing equations (10)–(12). Figure 5 shows the streamtraces for the FHD ($N = 0$) driven lid cavity flow for $Mn_F = 64.09$, 256.35 and 512.70, respectively. Initially, the application of the magnetic field results to the generation of single minor vortex for $0.42 \lesssim x \lesssim 0.5$ and for $0 \lesssim y \lesssim 0.05$ (see Fig. 5(A)). For this lowest value of Mn_F the vortices at the two bottom corners of the cavity remain unaffected com-

pared to the hydrodynamic case (Fig. 2). As the magnetic number Mn_F increases (Fig. 5(B)) the vortex generated by the applied magnetic field is extended. For $Mn_F = 256.35$ two clockwise rotating vortices are formed at the area of the lower left corner. Finally, with the increment of the magnetic field strength and for $Mn_F = 512.70$ one major vortex is formed for $x < 0.5$ and $y < 0.3$ (see Fig. 5(C)). It is also observed from the three Figs. 5 that the major vortex formed in the bottom right corner for hydrodynamic flow, remain unaffected regardless the strength of the applied magnetic field. Moreover, the vortex formed at the area of the magnetic source is always terminated directly above the location of the source and extends to the left side only. This way of formation of the vortex at the area of the application of the magnetic field is a classical effect of the FHD force observed also in [1, 23, 24] and [31].

The MHD driven lid cavity flow ($Mn_F = 0$) is shown at Fig. 6 for $N = 1.56 \times 10^{-3}$, 2.50×10^{-2} and 0.1, respectively. It is observed that the velocity flow fields pictured at Fig. 6 are almost identical with the corresponding ones of BFD flow pictured at Fig. 4. From Figs. 4(A) and 6(A) it is obtained that the contribution of the FHD force is the braking of the minor vortex at the area $0.4 \lesssim x \lesssim 0.6$ and for $0 \lesssim y \lesssim 0.8$ (Fig. 6(A)) to three others even smaller vortices occupying almost the same area (Fig. 4(A)). Similar phenomenon is observed at Figs. 4(B) and 6(B) where the stable minor vortex at the area $0.44 \lesssim x \lesssim 0.6$ and $y \lesssim 0.3$ (Fig. 6(B)) is braking to two barely distinguished vortices at the same area (Fig. 4(B)). Analogous results are observed comparing Figs. 4(C)–6(C) regardless the increment of the applied magnetic field.

Clearly, the velocity field of the BFD flow is formed mainly by the contribution of the MHD principles for the current form of the applied magnetic field and the FHD forces influence a very small area close to the magnetic source. It is noticed that the FHD forces alone, are not negligible comparable to the hydrodynamic case and play important role for the determination of the velocity field (Fig. 5).

4 Concluding remarks

The biomagnetic (blood) fluid flow in a lid driven cavity is studied. The numerical solution of the problem is obtained by the development of an efficient numerical technique based on the SIMPLE algorithm.

The derived results are presented in three sets. The first set correspond to the general BFD model (polarization and electrical conductivity are both taken into account), the second set for FHD model (polarization is taken into account) and the third set for MHD model (the electrical conductivity is taken into account).

For the first set, the results show that the application of the magnetic field at the area below the bottom plate of the cavity, result to the braking of the characteristic primary vortex of the pure hydrodynamic flow. For relatively weak magnetic field strengths, this braking leads to the formation of other smaller vortices which increase in number with the increase of the magnetic field strength. For relatively strong magnetic fields, the increased number of vortices results to the reduction of the velocities of the flow field close to the area of the bottom plate. For this set the application of the applied magnetic field creates disturbances all over the flow field.

The second set results indicate that the polarization force alone is significant and can influence the flow field by the formation of an extra major vortex comparable to the pure hydrodynamic case. For this case the influence of the magnetic field on the flow is local and is confined close to the area of application of the magnetic field.

The third set results, exhibit many similarities to those presented for the first set. For this specific physical problem, the contribution of the magnetic force due the electrical conductivity is mainly the factor that determines the final flow pattern rather than the force raised due to polarization. These numerical results could be useful in biomedical applications driving the flow of biological fluids either globally or locally close to the area of the magnetic field influence.

References

1. Haik Y, Chen JC, Pai VM (1996) Development of biomagnetic fluid dynamics. In: Winoto SH, Chew YT, Wijeysundera NE (eds) Proceedings of the IX international symposium on transport properties in thermal fluids engineering, Singapore, Pacific Center of Thermal Fluid Engineering, Hawaii, USA, June 25–28, pp 121–126
2. Haik Y, Pai V, Chen CJ (1999) Biomagnetic fluid dynamics. In: Shyy W, Narayanan R (eds) Fluid dynamics at interfaces. Cambridge University Press, Cambridge, pp 439–452
3. Bashtovoy VG, Berkovsky BM, Vislovich AN (1988) Introduction to thermomechanics of magnetic fluids. Hemisphere/Springer, Washington/Berlin

4. Berkovski B, Bashtovoy V (1996) Magnetic fluids and applications handbook. Begell, New York
5. Blums E, Cebers A, Maiorov MM (1997) Magnetic fluids. de Gruyter, Berlin
6. Fertman VE (1990) Magnetic fluids guidebook: properties and applications. Hemisphere, New York
7. Neuringer JL, Rosensweig RE (1964) Ferrohydrodynamics. Phys Fluids 7:1927–1937
8. Rosensweig RE (1985) Ferrohydrodynamics. Cambridge University Press, Cambridge
9. Rosensweig RE (1987) Magnetic fluids. Annu Rev Fluid Mech 19:437–463
10. Tzirtzilakis EE (2005) A mathematical model for blood flow in magnetic field. Phys Fluids 17:077103
11. Cramer KR, Pai SI (1973) Magnetofluid dynamics for engineers and applied physicists. Scripta, Washington
12. Hughes WF, Young FJ (1966) The electromagnetodynamics of fluids, 1st edn. Wiley, New York
13. Sutton GW, Sherman A (1965) Engineering magnetohydrodynamics. McGraw-Hill, New York
14. Davidson PA (2001) An introduction to magnetohydrodynamics. Cambridge University Press, Cambridge
15. Carlton JMR, Yowell CA, Sturrock KA, Dame JB (2001) Biomagnetic separation of contaminating host leukocytes from Plasmodium-infected erythrocytes. Exp Parasitol 97:111–114
16. Fuh CB, Lin LY, Lai MH (2000) Analytical magnetapheresis of magnetically susceptible particles. J Chromatogr A 874:131–142
17. Li XL, Yao KL, Liu ZL (2008) CFD study on the magnetic fluid delivering in the vessel in high-gradient magnetic field. J Magn Magn Mater 320:1753–1758
18. Voltairas PA, Fotiadis DI, Michalis LK (2000) Hydrodynamics of magnetic drug targeting. J Biomech 35:813–821
19. Haik Y, Pai V, Chen CJ (1999) Development of magnetic device for cell separation. J Magn Magn Mater 194:254–261
20. Takeda S, Mishima F, Fujimoto S, Izumi Y, Nishijima S (2007) Development of magnetically targeted drug delivery system using superconducting magnet. J Magn Magn Mater 311:367–371
21. Jordan A, Scholz R, Wust P, Fähling H, Felix R (1999) Magnetic fluid hyperthermia (MFH): cancer treatment with AC magnetic field induced excitation of biocompatible superparamagnetic nanoparticles. J Magn Magn Mater 201:413–419
22. Misra JC, Sinha A, Shit GC (2010) Flow of a biomagnetic viscoelastic fluid: application to estimation of blood flow in arteries during electromagnetic hyperthermia, a therapeutic procedure for cancer treatment. Appl Math Mech 31:1405–1420
23. Ganguly R, Gaind AP, Sen S, Puri IK (2005) Analyzing ferrofluid transport for magnetic drug targeting. J Magn Magn Mater 289:331–334
24. Loukopoulos V, Tzirtzilakis E (2004) Biomagnetic channel flow in spatially varying magnetic field. Int J Eng Sci 42:571–590
25. Misra JC, Shit GC (2009) Flow of a biomagnetic Visco–Elastic fluid in a channel with stretching walls. Trans ASME J Appl Mech 76:061006
26. Bhargava R, Bég AO, Sharma S, Zuecoc J (2010) Finite element study of nonlinear two-dimensional deoxygenated biomagnetic micropolar flow. Commun Nonlinear Sci Numer Simul 15:1210–1223
27. Misra JC, Shit GC (2009) Biomagnetic viscoelastic fluid flow over a stretching sheet. Appl Math Comput 210:350–361
28. Bég OA, Takhar HS, Bhargava R, Sharma S, Hung T-K (2007) Mathematical modeling of biomagnetic flow in a micropolar fluid-saturated Darcian porous medium. Int J Fluid Mech Res 34:403–424
29. Bég OA, Bhargava R, Rawat S, Halim K, Takhar HS (2008) Computational modelling of biomagnetic micropolar blood flow and heat transfer in a two-dimensional non-Darcian porous medium. Meccanica 43:391–410
30. Takhar HS, Bhargava R, Rawat S, Beg TA, Bég OA, Hung T-K (2007) Biomagnetic hydrodynamics in a 2-dimensional non-Darcian porous medium: finite element study. J Theor Appl Mech 37:59–76
31. Tzirtzilakis EE (2008) A simple numerical methodology for BFD problems using stream function vorticity formulation. Commun Numer Methods Eng 24:683–700
32. Ghia U, Ghia KN, Shin CT (1982) High-Re solutions for incompressible flow using the Navier–Stokes equations and a multigrid method. J Comput Phys 48:387–411
33. Erturk E (2009) Discussions on driven cavity flow. Int J Numer Methods Fluids 60:275–294
34. Kalita JC, Gupta MM (2010) A streamfunction-velocity approach for 2D transient incompressible viscous flows. Int J Numer Methods Fluids 62:237–266
35. Spotz WF (1998) Accuracy and performance of numerical wall boundary conditions for steady, 2d, incompressible streamfunction vorticity. Int J Numer Methods Fluids 28:737–757
36. Früh WG (2005) Using magnetic fluids to simulate convection in a central force field in the laboratory. Nonlinear Process Geophys 12:877–889
37. Früh WG (2005) Heat transfer enhancement by thermomagnetic convection. In: Jansens, P, Stankiewicz, A., Green, A (eds) Sustainable (bio)chemical process technology—incorporating the 6th international conference on process intensification. BHR, Cranfield, pp 47–56
38. Ece MC, Büyük E (2007) Natural convection flow under a magnetic field in an inclined square enclosure differentially heated on adjacent walls. Meccanica 42:435–449
39. Kumar N, Gupta S (2012) MHD free-convective flow of micropolar and Newtonian fluids through porous medium in a vertical channel. Meccanica 47:277–291
40. Abo-Dahab SM (2012) Effect of magneto-thermo-viscoelasticity in an unbounded body with a spherical cavity subjected to a harmonically varying temperature without energy dissipation. Meccanica 47:613–620
41. Jue T-C (2006) Analysis of combined thermal and magnetic convection ferrofluid flow in a cavity. Int Commun Heat Mass Transf 33:846–852
42. Ashouri M, Ebrahimi B, Shafii MB, Saidi MH, Saidi MS (2010) Correlation for Nusselt number in pure magnetic convection ferrofluid flow in a square cavity by a numerical investigation. J Magn Magn Mater 322:3607–3613
43. Farahbakhsh I, Ghassemi H (2010) Numerical investigation of the Lorentz force effect on the vortex transfiguration in a

two-dimensional lid-driven cavity. Proc Inst Mech Eng C: J Mech Eng Sci 224:1217–1230
44. Tannehill JC, Anderson DA, Pletcher RH (1997) Computational fluid mechanics and heat transfer, 2nd edn. Taylor & Francis, London
45. Harlow FH, Welch JE (1965) Numerical calculation of time-dependent viscous incompressible flow of fluid with free surface. Phys Fluids 8:2182
46. Ferziger JH, Perić M (2002) Computational methods for fluid dynamics, 3rd edn. Springer, Berlin
47. Fletcher CAJ (1991) Computational techniques for fluid dynamic, vol II, 2nd edn. Springer, Berlin
48. Patankar SV (1980) Numerical heat transfer and fluid flow. McGraw-Hill, New York
49. Pedley TJ (1980) The fluid mechanics of large blood vessels. Cambridge University Press, Cambridge
50. Gabriel S, Lau RW, Gabriel C (1996) The dielectric properties of biological tissues: III. Parametric models for the dielectric spectrum of tissues. Phys Med Biol 41:2271–2293
51. Frewer RA (1974) The electrical conductivity of flowing blood. Biomed Eng 9:552–554